Electronic Supplementary Information

Flexible copper wires through galvanic replacement of zinc paste: A highly cost-effective technology for wiring flexible printed circuits

Jingping Liu, Cheng Yang,* Peichao Zou, Rui Yang, Chao Xu, Binghe Xie, Ziyin Lin, Feiyu Kang, and Ching Ping Wong

Content

1. The investigation of the galvanic replacement conditions

1.1 The influence of pH value.

It is known that pH value plays a key role in the kinetics of the galvanic replacement reaction. In order to better understand the process, we measured the electrical resistivity of the replaced Cu (p-Cu) layer by four-point probe method. As shown in figure S1, the g-Cu film shows the lowest electrical resistivity when the pH was 1.5. The corresponding microscopic photographic images are shown in figure S2.

The samples were immersed into a $CuSO_4$ aqueous solution with different pH values, until the galvanic replacement process was automatically terminated (after about 20 minutes). The pH value was 3.7 for the pure $CuSO_4$ solution, as shown in figure S2 b), we can observe that only a little g-Cu were capped on the Zn particles. When we decreased the pH value by using H_2SO_4, more g-Cu was deposited as shown in figure S2 c) (pH = 2.0). When the pH value was reduced to 1.5, the deposited Cu formed a uniform continuous layer. When we decreased the pH value further, the g-Cu layer became sparsely distributed, as shown in figure S2 f); which was because Zn is too rapidly dissolved due to the presence of H^+ before it reacted with Cu^{2+}.

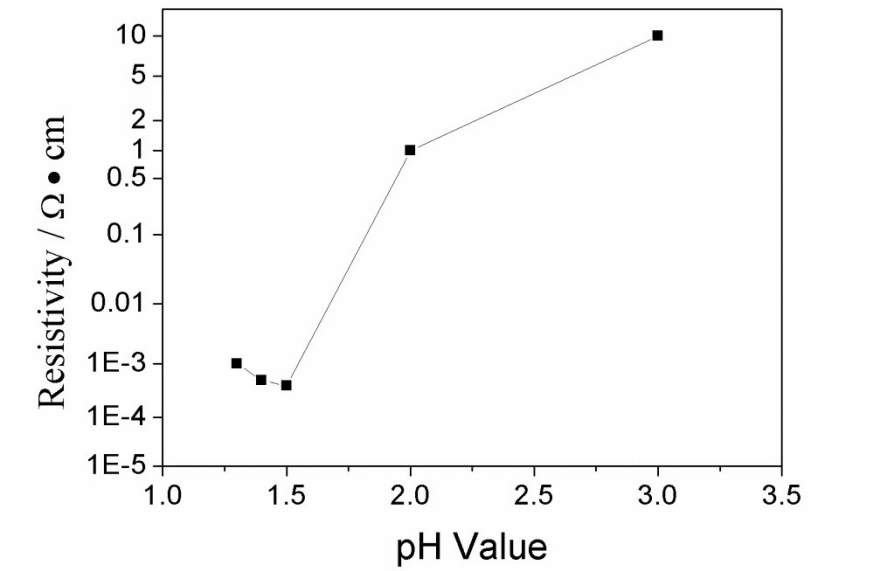

Figure S1 The electrical resistivity of the galvanic replacement deposited Cu (g-Cu) layer at different pH value.

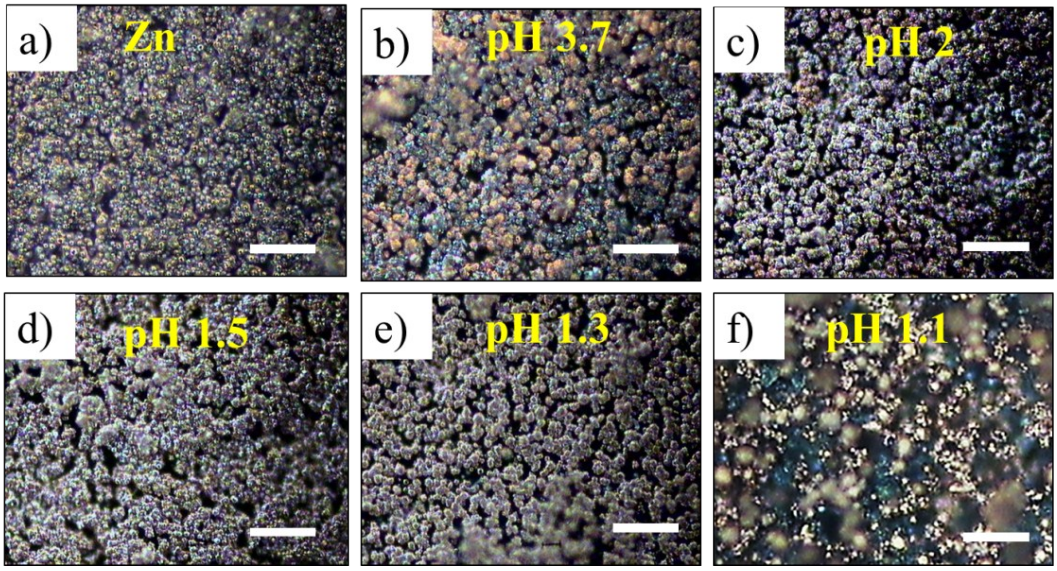

Figure S2 Optical microscopic images of the replacement deposited Cu (g-Cu) at different pH value. The scale bars are all 5 μm.

1.2 The influence of PEG.

The presence of poly(ethylene glycol) (PEG) can help to modulate the replacement reaction kinetics. A proper amount of PEG can adjust the grain size of the deposited Cu, which is important for the formation of a uniform g-Cu layer. Figure S3 series show some of the selected microscopic images of the sample with different concentrations of PEG (Mw = 4000). Figure 3 a) shows the sample without using PEG, figure S3 b) shows the image of the sample with 0.1% by weight of PEG. As compared, increasing the PEG concentration up to 1% and 10% respectively resulted in the vertical growth of the g-Cu grains, which was disadvantageous to form a uniform g-Cu layer. As a result, the electrical resistivity increased to the level of $10^{-2}\Omega\cdot$cm at the 1% PEG ratio and 10 $\Omega\cdot$cm at the 10% PEG ratio.

Based on a series of careful observations and optimizations of the reaction parameters, we selected the pH value of 1.5 and PEG surfactant content of 0.1% in the following experiments.

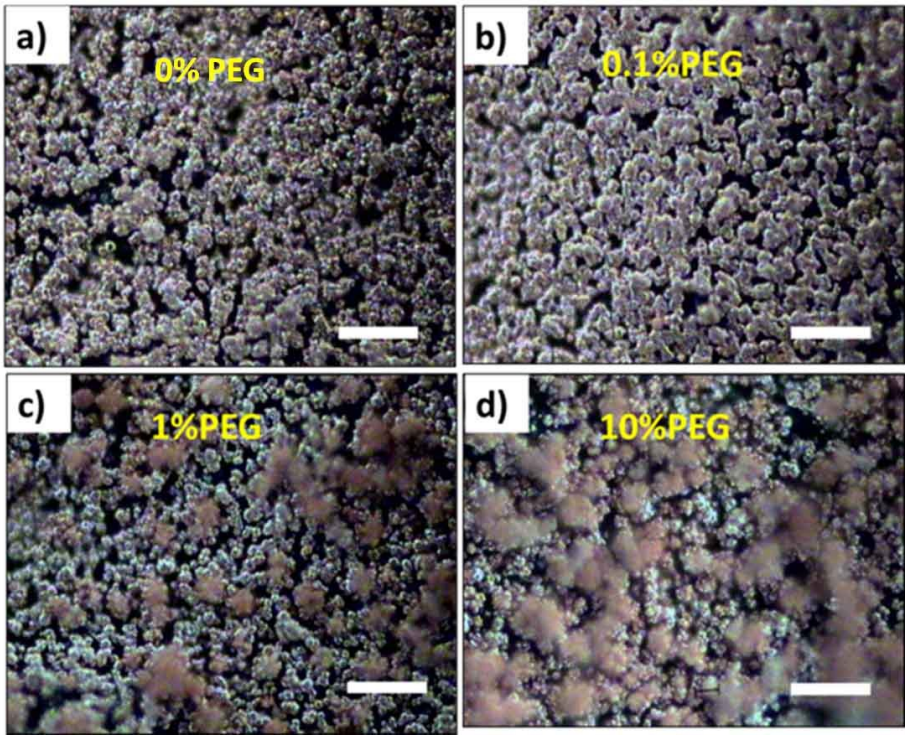

Figure S3 Optical microscopic images of the surface of the replacement deposited Cu at a) 0% PEG; b) 0.1% PEG; c) 1% PEG; d) 10% PEG; the pH value is 1.5. The scale bars are 0.5 μm.

2. Electroplating of Cu.

The receipt of the electroplating solution is listed in table S1. The anode was a phosphor copper plate; the current density of cathode was 10 mA/cm^2. The plating time was 5-30 min to modulate the thickness of the p-Cu.

Table S1 the main components of the electroplating solution.

Components	Content
$CuSO_4$	1.25 mol/L
H_2SO_4	0.6 mol/L
NaCl	2.4 mol/L
Brightener (BASF 910)	2-6 mL/L
PEG4000	0.1 mmol/L

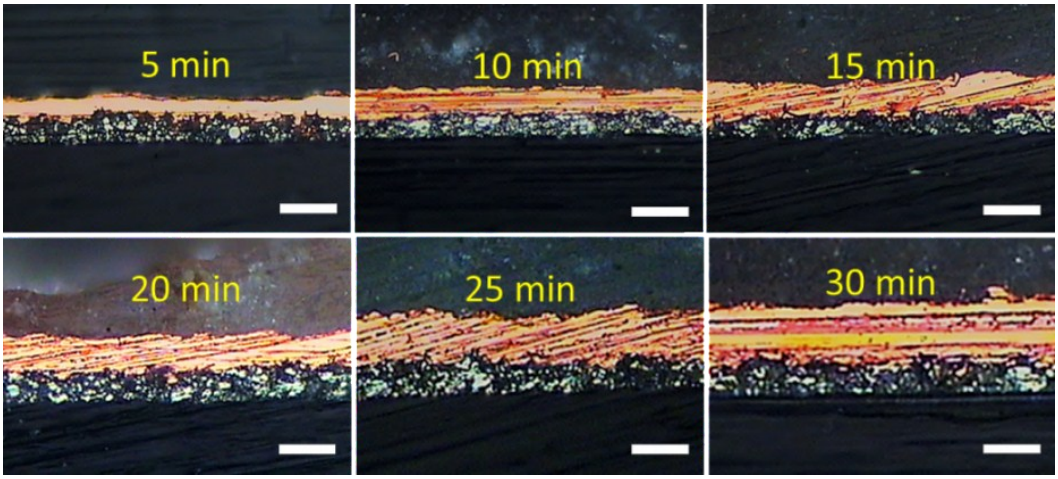

Figure S4 The optical microscopic images of the cross section of the electroplated Cu (p-Cu) layer at different plating time. All scale bars are 20 μm.

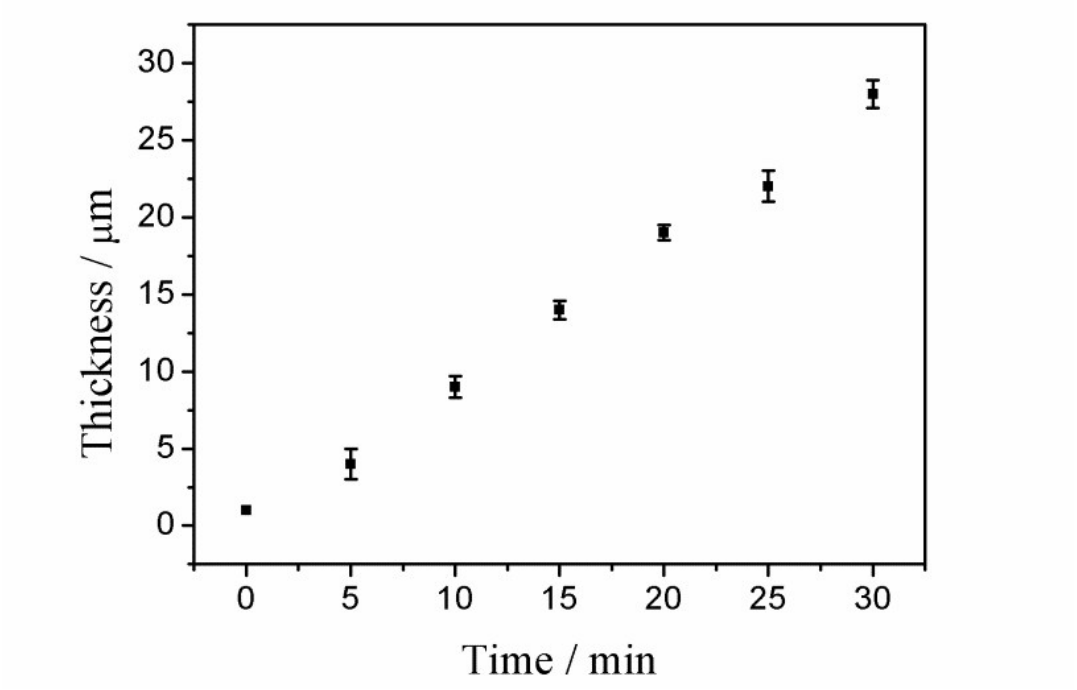

Figure S5 The relationship of the thickness of the p-Cu layer at different plating time.

From figure S4 and S5, we can see that the thickness of the electroplated Cu (p-Cu) layer had an approximate linear correlation with the plating time. The corresponding current density was 10 mA/cm^2.

3. Elemental analysis.

Figure S6 shows the TEM images of the Zn nanoparticles involved in this work. The size is about 50 nm and the surface is clean.

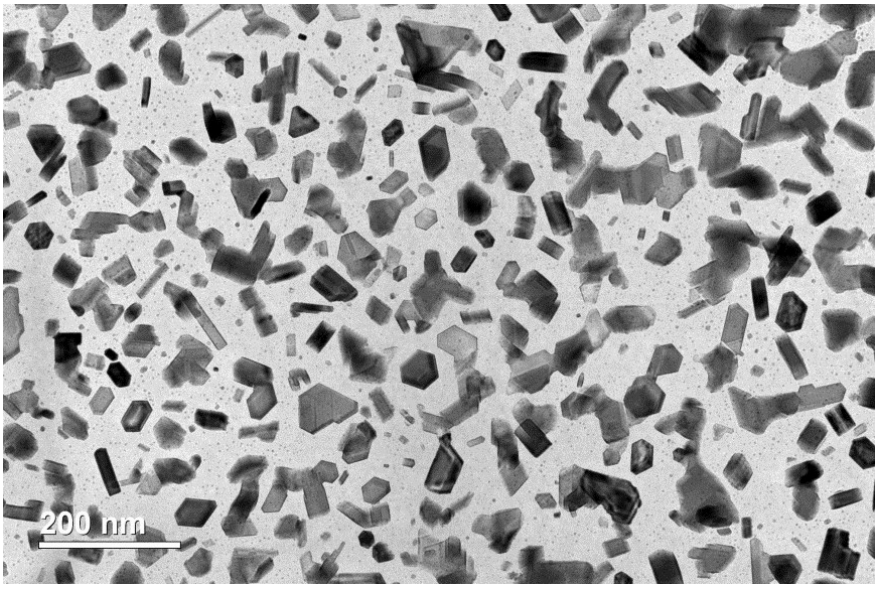

Figure S6 TEM images of the Zn nano particles

Figure S7 shows the cross sectional SEM images and element distribution of the printed Zn paste before and after galvanic replacement deposition of g-Cu. From figure S7 a) and c) we can see that after replacement, a thin layer of Cu formed on the surface of the printed Zn paste which was about 1 μm thick. From the corresponding elemental distribution analysis shown in figure S7 d) we can see that this thin layer is Cu (section I). Meanwhile, from figure S7 d) we can observe that in the near surface area which is marked as section II, the distribution of Zn element is less than the deeper part in section III, which means that the Zn on the surface of the printed Zn paste was depleted and replaced by Cu. What's more, the SEM image of figure S7 c) also shows a good combination between the g-Cu layer and the epoxy resin. Figure S7 e) and f) are the EDS spectrum of b) and d).

Figure S8 presents the XRD patterns of the samples in different steps. By comparison with the PDF card, we found that the XRD diffraction pattern matched well with the PDF standard card of Zn (No.04-0831), as marked in figure S8, the diffraction peaks

around 2 θ =25.9° may present the epoxy resin in the Zn paste. The diffraction peaks of Cu (PDF No. 04-0836) appeared after the galvanic replacement deposition process, indicating the thin layer of Cu that deposited on the top of the Zn paste. After the Cu layer was thickened with electro-plating (20min), the Cu layer was too thick (about 20 μm) that there was only diffraction peaks of Cu left.

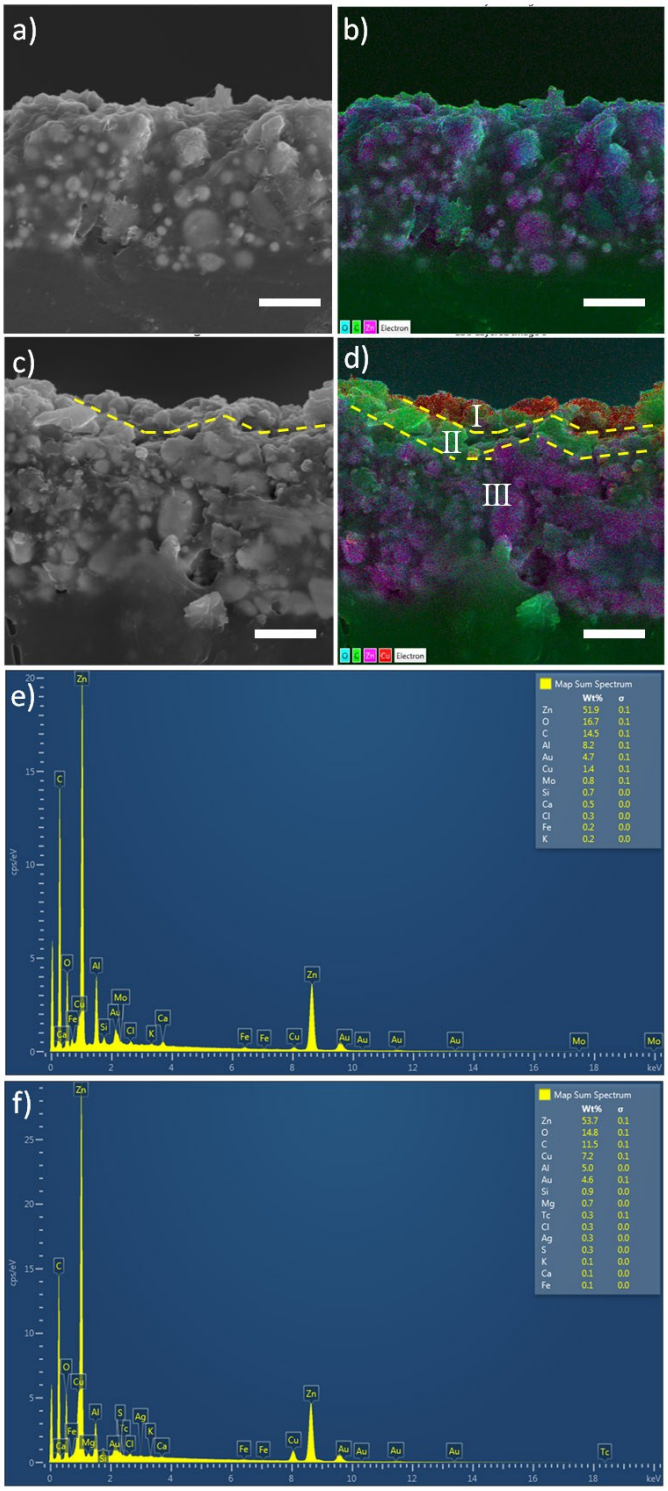

Figure S7 a) SEM image of the cross section of the printed Zn/epoxy paste before the galvanic replacement deposition of g-Cu. b) SEM-EDS mapping of a). c) SEM image of the cross section of the printed Zn/epoxy paste after replacement deposition of Cu. d) SEM-EDS mapping of c). e) the EDS spectrum of the whole are in b); f) the EDS spectrum of the whole area in d); The scale bars are 5 μm.

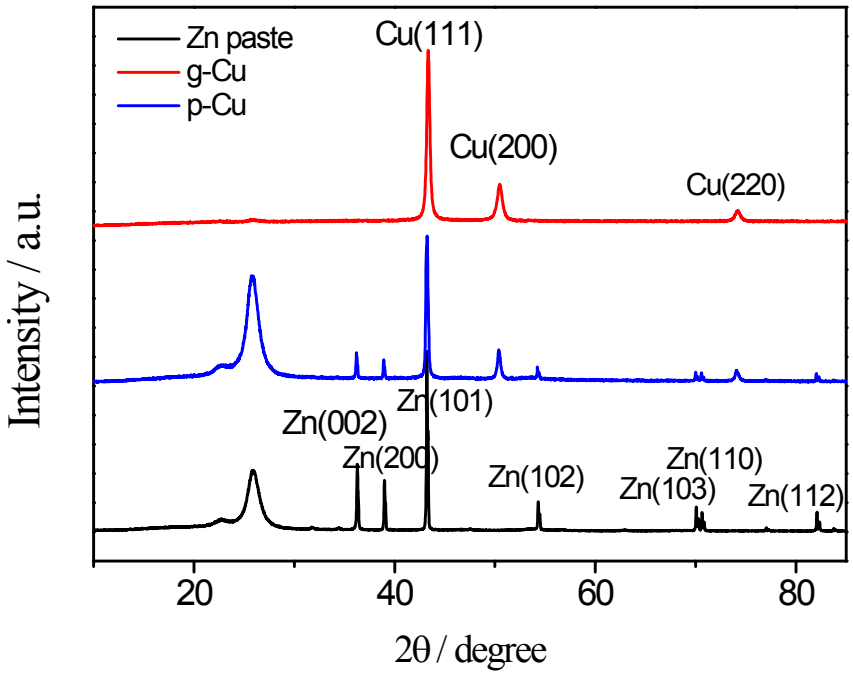

Figure S8 XRD patterns of the printed Zn paste, g-Cu and p-Cu layer.

4. Lap-shear measurement and fractography analysis.

In order to evaluate the adhesion strength of the copper layer on the substrate, we conducted the lap-shear test on a tensile tester. The sample was measured as shown in the schematic in figure S9; the p-Cu pads were 8 mm × 10 mm and were pasted face to face with ethyl -alpha-cyanoacrylate glue (No.502 glue). Then the samples were pulled apart. The result is shown in figure S10; the maximum tensile force was 8.45 N, which suggested a shear stress of 0.105 MPa.

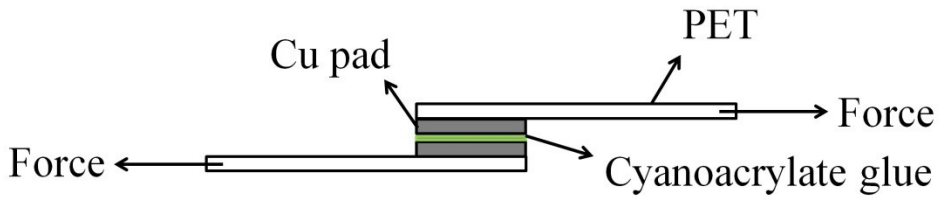

Figure S9 the schematic of the shear stress measurement.

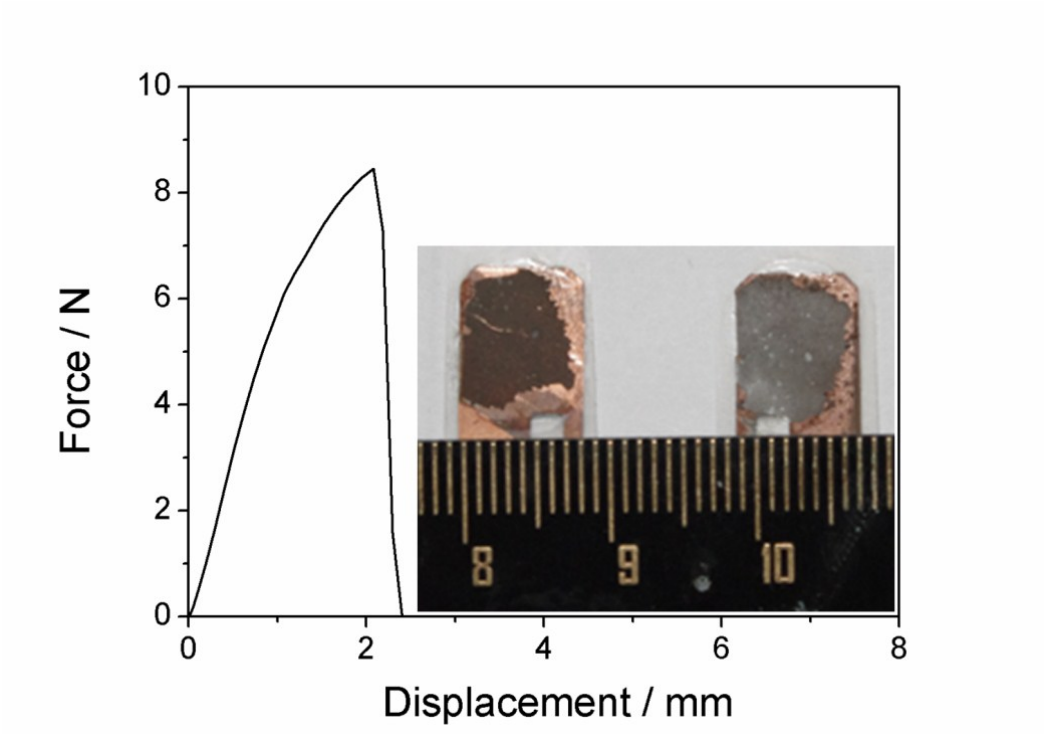

Figure S10 The force vs displacement in the shear stress measurement. The insert is the photo of the samples after the measurement.

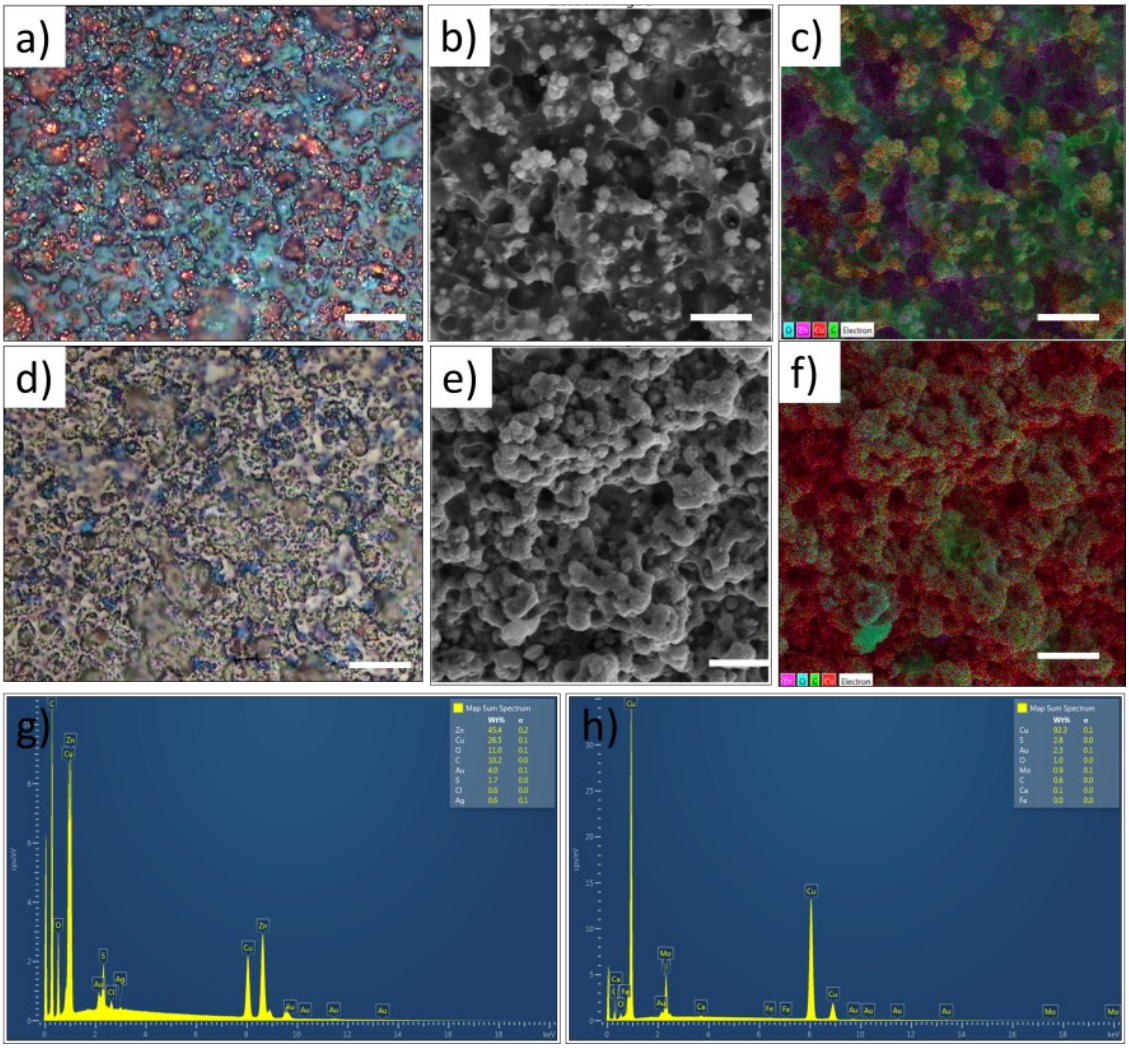

Figure S11 The morphology and elemental analysis of the fracture surfaces after the lap-shear test. a) The optical microscope image of the epoxy/Zn side. b) the SEM image of the epoxy/Zn side; c) the SEM-EDS mapping of the epoxy/Zn side; d) The optical microscope image of the p-Cu layer side; e) the SEM image of the p-Cu layer side; f) the SEM-EDS mapping of the p-Cu layer; g) the EDS spectrum of map in c); h) the EDS spectrum of map in f). The scale bars of a) and d) are 50 μm; the scale bars of b), c), e) and f) are 5μm.

Optical microscopic inspection of the fracture surface shows that the Cu-epoxy interface is the weakest, as shown in figure S11. After the p-Cu layer was pulled off the substrate, there were still many Cu clusters inlayed in the epoxy resin, as shown in figure S11 a); furthermore, the SEM image and the elemental analysis in figure S11 b),

c) and g) showed the distribution of Cu in the epoxy layer. Also, on the p-Cu layer side, we can observe the epoxy residue and the rough surface as shown in figure S11 d), the SEM-EDS analysis in figure S11 e), f) and h) showed that a few C, O and Zn were distributed on the Cu surface, which represent the epoxy/Zn complex inserted in the Cu layer. The existence of epoxy residue is also confirmed by figure S11 d), as shown as the blue dots. Therefore, the interpenetration phenomenon is beneficial in improving the bonding between the p-Cu layer and the substrate through the mechanical interlocking effect.

5. Reliability test.

We conducted the reliability test for the samples by aging them in an accelerated aging chamber. The results are shown in both figure S12 and figure S13, in which the normalized resistance R/R_0 remains stable through the tests. Figure S12 is the aging test result of the sample in an 85°C/85 relative humidity (RH) testing chamber after 500 hours. Figure S13 is the aging test result of the sample in a thermal shocking chamber with -40°C to 125°C cyclings (every 60 minutes for one full thermal cycle). Both tests indicate a reliable performance of the circuit samples in severe working environments.

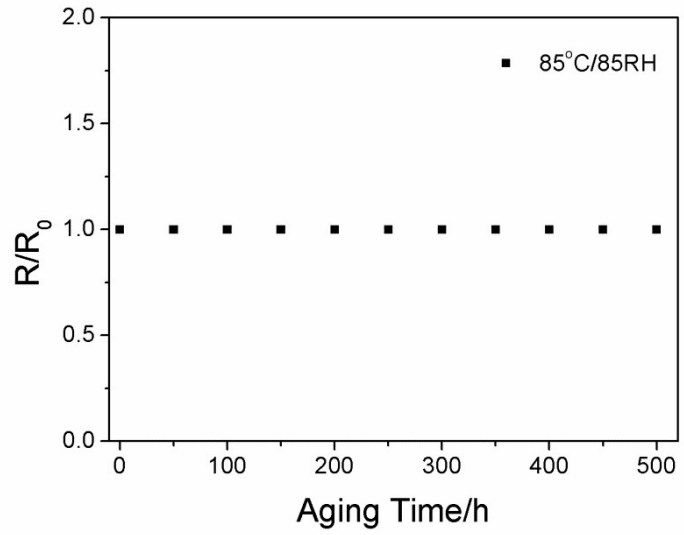

Figure S12 Constant temperature and humidity test of the p-Cu: normalized resistance R/R_0 vs. aging time.

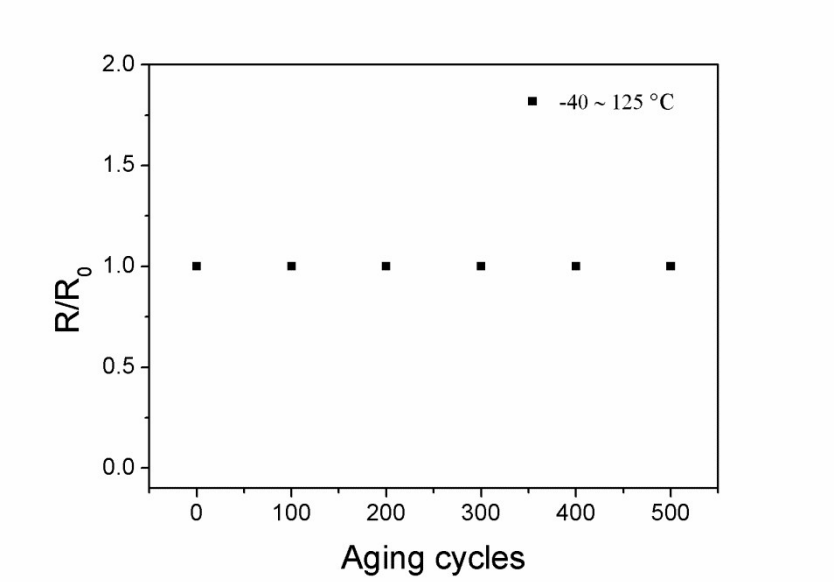

Figure S13 the thermal shocking test of the p-Cu: normalized resistance R/R_0 vs. aging time.

6. FTIR analysis of the Zn/epoxy paste.

Figure S14 and S15 show the Fourier Transform infrared spectroscopy (FTIR) analysis of both the cured pure epoxy resin and the Zn/epoxy paste. There are many oxygen functional groups on the cured epoxy surface; as for the Zn/epoxy paste, the FTIR peaks of the oxygen functional groups became weak because the Zn particles react with the oxygen functional groups. When the Zn nanoparticles are replaced by Cu, and these oxygen functional groups can interact with the Cu metal, as the previous investigations reported that Cu-O-C complex may form in the interface of the p-Cu layer and the epoxy resin.[1-4] The interaction between the p-Cu metal layer and the substrate can partially attribute to the improvement of adhesion strength.

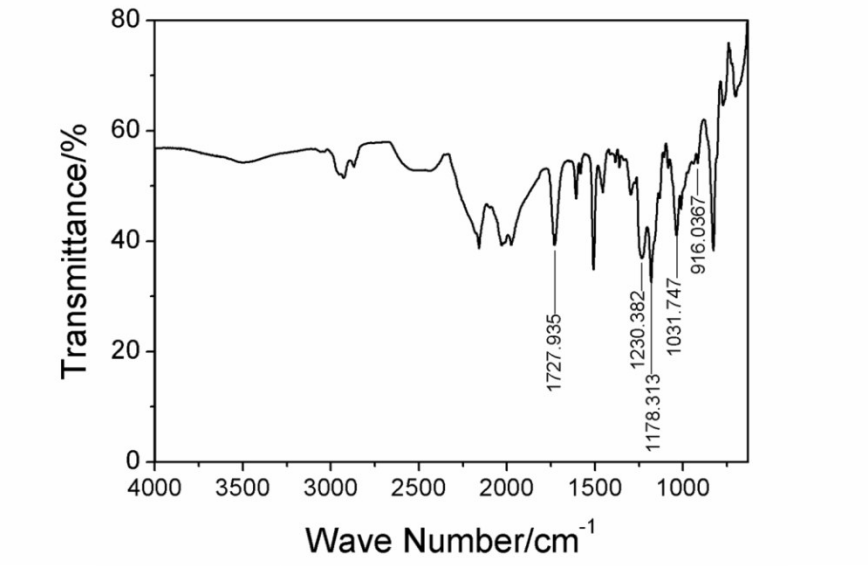

Wave number/cm^{-1}	Functional group	Wave number/cm^{-1}	Functional group
916.0367	C−C (O)	1031.747 1178.313	C-O-C
1230.382	C-O	1727.935	C=O

Figure S14 The FTIR spectrum of the cured epoxy resin.

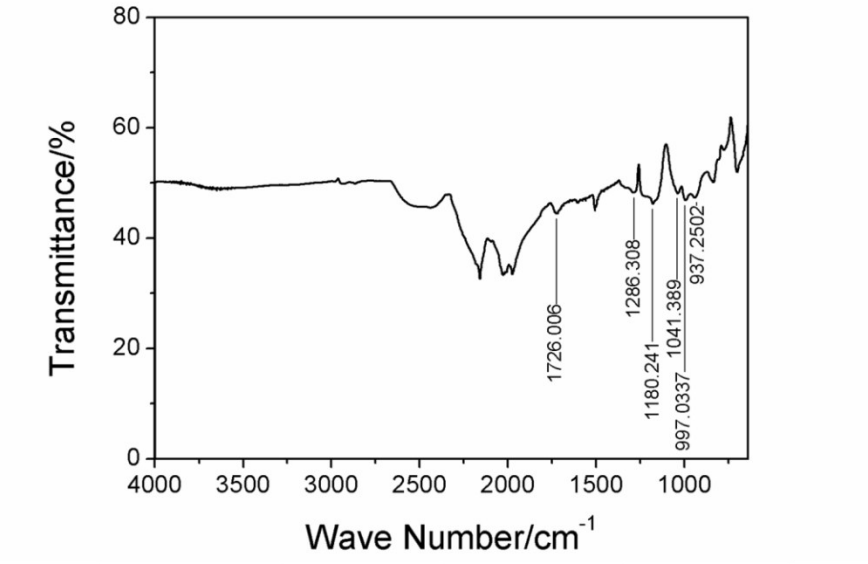

Wave number/cm^{-1}	Functional group	Wave number/cm^{-1}	Functional group
937.2502 997.0337	C−C (O)	1041.389 1180.241	C-O-C
1286.308	C-O	1726.006	C=O

Figure S15 The FTIR spectrum of the cured Zn/epoxy paste.

7. DSC-TG analysis of the epoxy resin.

The Differential Scanning Calorimetry-Thermal Gravity (DSC-TG) analysis was conducted in N_2 atmosphere at a heating rate of 5°C/min; the samples were epoxy resin and Zn/epoxy resin, respectively. From the result of epoxy resin as shown in figure S16, we can observe that an exothermic peak begins at 150°C, which means the starting of the curing process of the reaction of the epoxy resin and the curing agent. But the result of the Zn/epoxy shows an exothermic peak at lower temperature as shown in figure S17; which begins at about 118 °C, which means that the Zn/epoxy paste can be cured at a relatively lower temperature. This is beneficial for some substrates that are unable to bear high temperature.

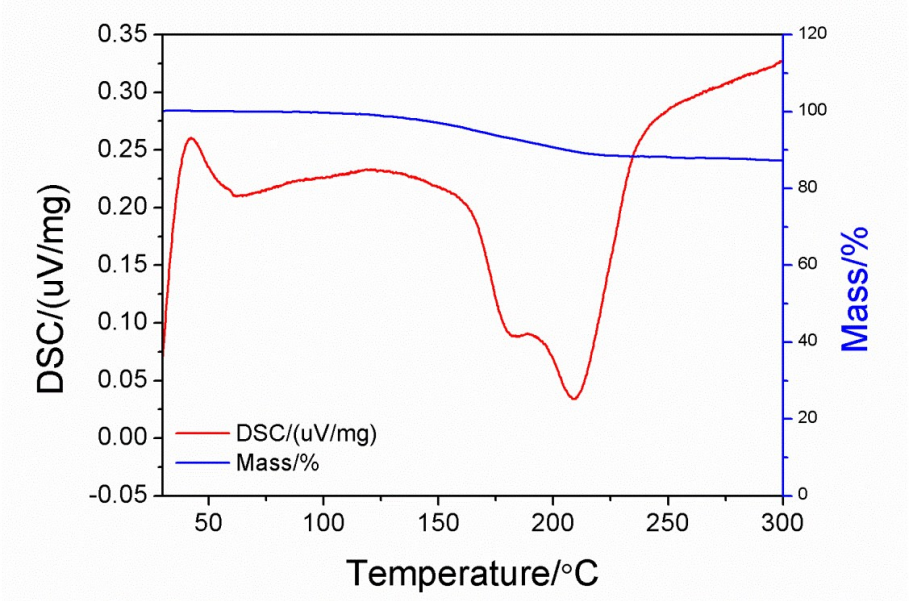

Figure S16 The DSC-TG measurement of the epoxy resin.

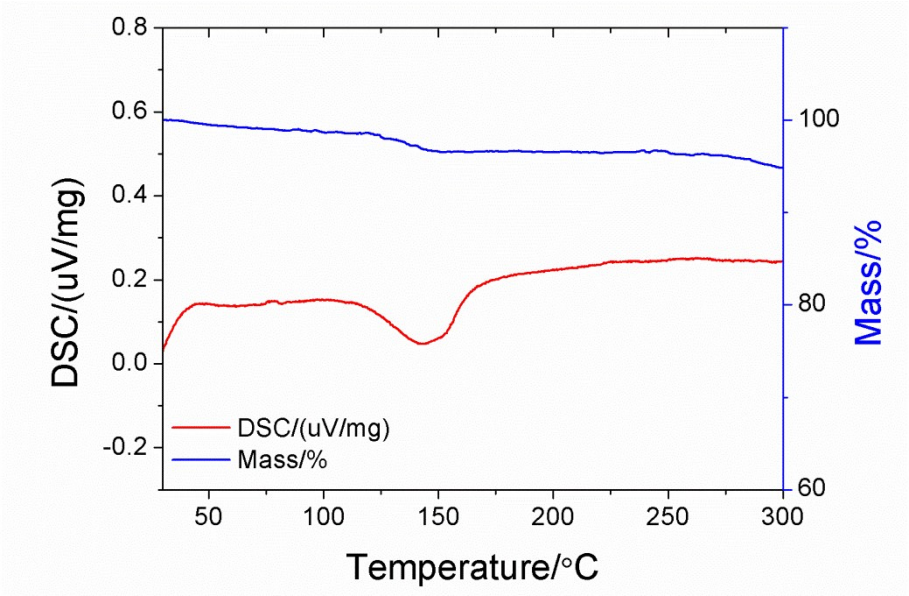

Figure S17 The DSC-TG measurement of the Zn/epoxy resin.

8. The performance test of the RFIDs.

In order to further evaluate the device performances using the p-Cu wired samples, we analyzed the read range performance of some radio frequency identification (RFID) tag samples. The antennas were fabricated with p-Cu (electro-plating time was 20 min), Al and Ag paste (75 wt% Ag), which were tested by an Invengo XCRF-800 reader at a transmitting power of 30 dBm. The Al based RFID tag is from Alien Co. The other samples were fabricated with the same antenna layout. All chips are the same.

Figure S18 shows the photographic images of the RFID tags. Table S2 is the comparison of the performance of the three kinds of RFID tags. Results suggest that the p-Cu based antenna material has the lowest electrical resistance; as compared, it has a similar signal transmittance distance to the commercial (Al based) one for the same chip. The Ag paste based antenna shows the shortest read range.

Table S3 is the comparison of various wiring technologies, compared with the complex processes of the conventional Cu etching technology, the techniques based on printing methods is more efficient and with less process cost, as for the Ag based printing electronic technology, the materials cost of Ag maybe the main limitation,

besides, the conductivity of printed Ag paste/ink is much lower. For the Cu wiring technologies, the electroless plating method may obtain finer circuits, but the electroless plating process always needs strict conditions because the plating solution is easy to loss the activity, what's more, the organic regents in the plating solution may cause environmental problems. In this case, the Cu wiring technology that based on Zn/Cu^{2+} replacement reaction has many advantages: the cost of materials is low, the Cu deposition process is simple and easy to operate and the performance of the as prepared Cu circuits is good enough.

Table S2 The properties of the RFID samples made in different technologies.

Antenna materials	p-Cu	Al	Ag paste
Pattern resistance	0.4Ω	0.7Ω	10.4Ω
Read range	~3.5m	~3.5m	~1.8m
Thickness	20 μm	15 μm	50 μm

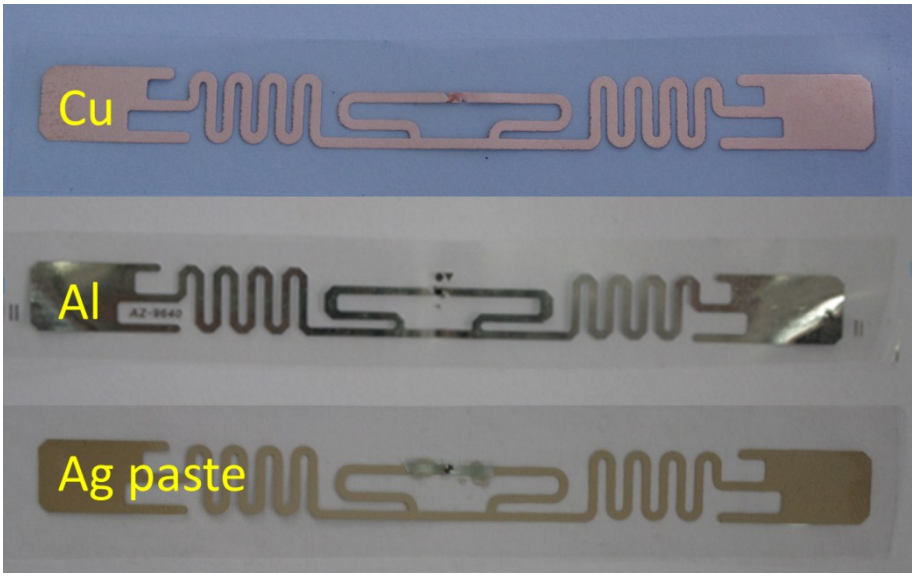

Figure S18 The RFID tags made with different technologies.

Table S3 comparison of different technologies

	Patterning	Pollutions	Cost	Resolution	Resistivity

	method				
Cu/Al etching	Photolithography	Serious	High	~50μm	~$1.7\times10^{-6}\Omega\cdot$cm
Ag based ECA	Screen printing, offset printing, gravure printing, pad printing, etc.	Little	High	~50 μ m (based on the printing technology)	~$10^{-5}\Omega\cdot$cm
Electroless plating	Inkjet printing, microconnect printing, etc.	Medium	Medium	~150μm	~$2\times10^{-6}\Omega\cdot$cm
Zn seed paste	Screen printing, offset printing, gravure printing, pad printing, etc.	Little	Low	~100μm (based on the printing technology)	~$1.7\times10^{-6}\Omega\cdot$cm

Reference

1. C. K. Y. Wong, M. M. F. Yuen and B. Xu, *Appl Phys Lett*, 2009, **94**, 263102.
2. W. J. Lee, Y. S. Lee, S. K. Rha, Y. J. Lee, K. Y. Lim, Y. D. Chung and C. N. Whang, *Applied Surface Science*, 2003, **205**, 128-136.
3. C. Wang, L. Xiang, Y. Chen, S. Wang, D. Xiao and W. He, *Journal of Adhesion Science and Technology*, 2015, 1-12.
4. W.-J. Liu, X.-J. Guo and C.-H. Chuang, *Surface and Coatings Technology*, 2005, **196**, 192-197.